coatings

MDPI

Article

Investigation of Tensile Properties at Room and Elevated Temperatures of S1100QL Steel and Its Welded Joints

Djordje Ivković [1,*], Dušan Arsić [1,*], Ljubica Radović [2], Nada Ilić [2], Jovana Mandić [2], Marko Delić [1] and Andjela Ivković [1]

[1] Faculty of Engineering, University in Kragujevac, 34000 Kragujevac, Serbia; marko.delic@kg.ac.rs (M.D.); andjamit99@gmail.com (A.I.)
[2] Military Technical Institute, 11030 Belgrade, Serbia; ljubica.radovic@vti.vs.rs (L.R.); nadalic67@gmail.com (N.I.); jamandic96@gmail.com (J.M.)
* Correspondence: djordje.ivkovic@fink.rs (D.I.); dusan.arsic@fink.rs (D.A.)

Abstract: The aim of this paper was to present an experimental study into the influence of elevated temperatures on the tensile properties of the ultra-high-strength steel (UHSS) S1100QL and its welded joints. S1100QL steel belongs to the group of structural steels, and it is mainly used for designing various types of lifts and cranes with the goal of decreasing the mass of structures while increasing their load capacity. Since the structures mentioned are mostly produced as welded structures, tensile tests were also conducted on the specimens prepared from two different types of welded butt joints made of S1100QL steel. One plate was welded with a preheating temperature of approx. 175 °C with a similar undermatching filler material, and the second plate was welded with slight preheating and with two different filler materials. For the root pass, an austenitic filler material was used, and for further passes the same undermatching filler material as in the first case was used. The goal of this study was to determine the highest temperature at which the steel and its welded joints maintain their properties. The first set of tensile tests focused on testing the properties of the base material at room and seven other elevated temperatures (from 100 °C to 700 °C). The results obtained showed that between 400 °C and 500 °C, properties begin to drop. The second set of tests focuses on investigating the tensile properties of S1100QL welded joints, both at room and elevated temperatures. In this paper, details on the welding technologies used and the microstructures obtained are also presented.

Keywords: S1100QL; tensile tests; elevated temperature; welded joints; microstructure

Academic Editor: Paolo Castaldo

Received: 28 April 2025
Revised: 31 May 2025
Accepted: 6 June 2025
Published: 9 June 2025

Citation: Ivković, D.; Arsić, D.; Radović, L.; Ilić, N.; Mandić, J.; Delić, M.; Ivković, A. Investigation of Tensile Properties at Room and Elevated Temperatures of S1100QL Steel and Its Welded Joints. *Coatings* **2025**, *15*, 696. https://doi.org/10.3390/coatings15060696

1. Introduction

It is well known that steel nowadays is one of the most used structural materials due to its superior properties such as strength and hardness and its ability to maintain these properties at elevated temperatures. Conventional steels have been used in industry for 150 years. Steel parts have allowed for an increase in the working range of parts and the durability of structures. As time passed, the application of steel parts expanded even more and with it the conditions that steel parts had to meet. Accordingly, various studies began to be carried out in the field of steel metallurgy. The aim was to enable steel materials to meet these various conditions established in the industry. For example, in 1913, corrosion-resistant steels were established as a result of a study in which the percentage of chromium in the properties of steel was investigated [1]. Over time, new requirements have emerged for increasing the load-bearing capacity of steel structures while simultaneously reducing their weight due to climate change and high carbon emissions. This has been particularly

emphasized in the automotive and transportation industries, where reducing the weight leads to lower fuel consumption. Due to that requirement, steel alloys had to evolve in a way that achieved greater strength, to withstand greater loads with smaller weight. This allowed for an increase in the load-bearing capacity of structures or a reduction in the mass of the structure and resulted in the discovery of high-strength steel (HSS), advanced high-strength steel (AHSS), and ultra-high-strength steel (UHSS).

Besides the transportation industry and structural applications, UHSS is very often used for protective purposes to make fire barriers in buildings where there is an increased risk of fire [2,3]. The aim of this paper is to investigate the tensile and metallurgical properties of UHSS structural S1100QL steel and its butt-welded joints at room and elevated temperatures.

Many studies devoted to the investigation of tensile properties at elevated temperatures already exist in the literature [4–6]. Studies have been conducted on different materials where examination temperatures, heating regimes, and other conditions were changed so that their influence on the materials' behavior could be assessed.

In their paper, Pang et al. [2] investigated the fire resistance of high-strength steel (HSS) H-section columns subjected to axial compression through comprehensive experiments and finite element analyses using three steel grades (Q460, Q690, Q960) with different load ratios and slenderness ratios under fire conditions. The experimental results show that increasing the load ratio from 0.3 to 0.5 reduces the critical temperature by approximately 10%–14%, while increasing slenderness ratios from 63 to 93 raises the critical temperature by around 6%–7%.

Qiang et al. [3], similar to Pang et al., investigated the behavior of high-strength steel (HSS) columns subjected to elevated temperatures through a combination of experimental tests and numerical modeling. The authors conducted compression tests on columns made of S460 and S690 steel grades at temperatures up to 900 °C. The test results showed reductions in strength and stiffness with increasing temperature, particularly above 600 °C.

As one of the more important studies, Neuenschwander et al.'s paper [4] examined how elevated temperatures affect the mechanical properties of butt-welded joints in the high-strength steels S700MC, S960QC, and S1100QC. In this study, steady-state tensile tests on both the base metal and welded joints were used, covering temperatures up to 900 °C. The results showed that welded joints of higher-strength steels like S960 and S1100 exhibit greater strength degradation compared to their base metals at elevated temperatures.

Lazic et al. [6] investigated the influence of temperature on the properties of structural steel S690QL and its welded joints. The examination temperature ranged from 20 °C to 550 °C. The study shows that the properties of the base material start to degrade at temperatures above 450 °C, and the properties of welded joints start to degrade at exactly 450 °C.

Arsic et al. [7] conducted a numerical analysis of the results obtained in [6]. Their numerical study shows a high correlation with the experimental study. The numerical results confirm that 450 °C indeed is the critical temperature. In another similar study, Arsic et al. [8] investigated the mechanical properties of hot-work steel H11 (AISI) at elevated temperatures. In this study, the examination temperature ranged from 20 to 700 °C. Within this study, both experimental and numerical methods were applied. The results of this study show that the properties of hot-work tool steel H11 are stable up to temperatures of 500 to 550 °C. At 600 °C and above, the yield stress and ultimate tensile strength begin to degrade with a simultaneous increase in the material's plasticity. It can be concluded that this steel can be used with great reliability up to 550 °C. The numerical model prepared for this study can be considered satisfactory, since the experiments' results are similar to the numerical results.

Other authors also dealt with the problem of tensile strength, as well with the welding of S1100 steel [9–13]. For instance, M. Ghafouri et al. [9] investigated the tensile properties

of S960MC, S1100, and their welded joints at elevated temperatures. In this paper, for both steels, just one welding technology was applied. As an extension of this work, this paper puts to the test two welding technologies that steel producers recommend.

Amraei et al. [10] examined the mechanical properties of butt-welded thin plates made of S700, S960, and S1100 steels under various heat inputs (HIs). They concluded that fracturing occurred in the base materials of all S700 and S1100 weldments, and S960 suffered from failure at the HAZ, which resulted in a reduction in the joint's strength and ductility.

Afkhami et al. [11,12] also examined the S1100 steel grade but as a study of the influence of cold forming on the weldability and fracture behavior of ultra-high-strength S1100 steel. The results confirmed the reliability of the welded joints in steel structures, and the fracturing of the welded material was identified as ductile, regardless of its cold-forming degree. Heat-affected zone softening, as a common drawback associated with welded ultra-high-strength steel, did not adversely affect the fracture mechanism of welded S1100, even in its cold-formed state.

Mandal et al. [13] investigated a low-carbon micro-alloyed steel containing high Ni and Cu content that had been developed and subjected to thermo-mechanical processing by varying the finish rolling temperature (850–750 °C) and cooling rates (air cooling and water quenching). After the process, they examined the microstructures of air-cooled samples in order to optimize the structure of the steel after the treatment. A satisfactory combination of tensile properties was achieved in as-cooled or as-quenched conditions (without the need for any tempering treatment).

Similar research was performed by Javidan et al. [14], where the topic of the research was determining the effect of welding on the mechanical properties of high- and ultra-high-strength tubes in hybrid sections, which is a critical factor that influences the global performance of fabricated members. To investigate and quantify these effects on the material of the welded steel, a specific type of hybrid section composed of plates and tubes was considered in which two scales of experimental analysis were conducted at different positions from the weld. At the macro-scale, standard tensile tests were performed at various distances from the weld to obtain the mechanical properties of the heat-affected steel in the axial direction parallel to the weld. At the micro-level, the microstructures of the three above-mentioned materials, in addition to microhardness profiles, were examined, providing extensive data on the materials' behavior after welding. It is shown that the welding and post-welding process, such as heat input and cooling rate, affect the local material properties at different distances from the weld, leading to an overall heterogeneity in the material influencing the mechanical behavior.

One of the most important research topics for these types of steel is crack growth under different loads. Moe et al. [15] performed an assessment of the fatigue crack growth rate behavior of welded structural components made of ultra-high-strength steels in order to gain a comprehensive understanding of these materials under high-cycle fatigue loadings and to enhance their applications in the construction industry. They concluded as follows: the hardness reduction in HAZ is minimal (about 4%) for S1100 steel, S1100 steel has a higher fatigue crack growth resistance than S700, and the crack growth behaviors in both WMs of SG960 and SG1100 were nearly similar due to the use of the same filler material for creating the weldments.

Since this steel grade is mainly intended for welded structures, it is very important to emphasize the role of welding and the selection of welding technology. It is very important to choose the right technology in order to obtain a welded structure of a certain integrity. That was the focus in [16,17], where investigation of the weldability of ultra-high-strength S1100QL steel was performed through hardness, impact toughness, and tensile strength testing. Using the MAG welding process with controlled parameters, high-quality welded

joints were achieved without the occurrence of cold cracks. The results show that impact toughness decreases with lower temperatures but remains within acceptable limits. The mechanical properties of the joints confirm good weld quality. The authors emphasize the importance of precise control over welding parameters, especially the cooling time $t_{8/5}$. This time refers to a cooling temperature interval between 800 and 500. This is the temperature interval of the least stability for austenite. The time spent in this interval for some steel grades can affect structures obtained at room temperature and consequently their mechanical properties.

Similar to previous authors, Liang et al. [18] also dealt with problems of UHSS welding and its properties after the welding. The introduction addresses the authors' intentions to research the tensile properties of the base metal and welded joints made of S1100 UHSS. Additionally, the literature currently shows a lack of investigation into the influence of temperature on the tensile properties of this steel.

S1100QL steel has extraordinary mechanical properties related to high strength (strength-to-weight ratio) but also good toughness. This steel is usually used for machine building, lifting equipment, fabricated towers, structural applications, agricultural systems, and combustible industries. Furthermore, S1100QL steel is used for the production of structures in flammable industries, which employ these plates for pipe production since they abate any leakages that can compromise safety standards. As previously mentioned, this group of steels is used for the production of fire protection plates in buildings, so its properties at elevated temperatures are extremely important [2–5]. Fire can be mentioned as among the most, if not the most, prominent catastrophic incidents to which structures are vulnerable, which can result in structural failure, followed by extreme consequences such as human fatalities, economic loss, and environmental pollution. Fire-safe designs and assessing the performance of steel structures made of HSSs and UHSSs exposed to fire conditions necessitate a profound understanding of the constitutive behavior of such materials at elevated temperatures. The aim of this research is to determine the mechanical properties of the base metal and welded joints of S1100QL steel at room and elevated temperatures, as well as to determine at which temperatures this steel loses its strength. In this paper, two welding technologies were tested. One was recommended by the steel producer, and the other was proposed by the authors, as it has been used in other research [9]. The reason for this was the steel producer recommends welding the S1100 steel according to procedure. However, the users of that steel often use welding technologies that differ from the proposed one, so we wanted to test two technologies. Furthermore, companies that buy welding steel generally do not have enough time to determine the most favorable welding technology but rely on the solutions offered by the manufacturer.

2. Materials and Methods

2.1. Base Material

For the purposes of this study on S1100QL, SSAB's STRENX 1100 E/F [19,20] was used for preparing specimens for both investigation of its tensile properties at room and elevated temperatures and for preparation of plates intended to be welded in the future, so that investigation of the welded joints' tensile and other properties could be conducted. As mentioned before, this steel belongs to the group of UHSS. Its mechanical properties and chemical composition declared by the producer are presented in Tables 1 and 2.

Table 1. Declared mechanical properties of S1100QL steel.

Yield Strength, $R_{p0.2}$, MPa	Tensile Strength, R_m, MPa	Elongation, A_5, %	Impact Toughness, $KV_{(-40)}$, J
min 1100	1250–1550	min 10	min 27

Table 2. Declared chemical composition.

%C	%Si	%Mn	%P	%S	%Cr	%Cu	%Ni	%Mo	%B
max 0.21	max 0.5	max 1.4	max 0.02	max 0.005	max 0.8	max 0.3	max 3	max 0.7	max 0.005

2.2. Introduction to Welding S1100QLl

For the purposes of this study, welding of S1100QL had to be conducted; since SSAB's STRENX 1100 E/F was used in this study, all the producer's available literature was consulted. For successful welding of STRENX 1100 E/F, SSAB recommends two different technologies, with and without preheating [19,20]. SSAB also gives recommendations regarding the heat input and filler materials that are used for both technologies. Four plates with dimensions of 200 mm × 500 mm × 12 mm were prepared, with the idea that two of them will obtain two welded joints where each technology will be applied. The plates were prepared and beveled for a V-butt joint. The prepared geometry is displayed in Figure 1, and recommendations regarding welding technology are displayed in Tables 3 and 4.

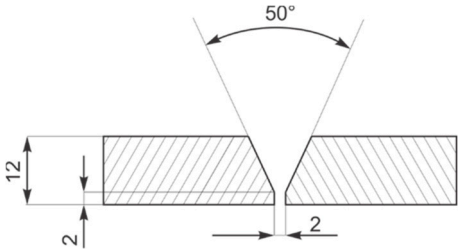

Figure 1. Sketch of beveled plates and prepared groove for welding.

Table 3. Recommendations for welding S1100QL without preheating [19,20].

		Technology A: Without Preheating	
Preheating Temperature		**Max 120 °C**	
Heat input		8–12 kJ/cm	
Filler materials	Root pass	G 18 8 Mn (according to EN 12072)	M12 shielding gas (according to ISO 14175)
	Filler passes	G 89 (according to EN ISO 16834)	M21 shielding gas (according to ISO 14175)

Table 4. Recommendations for welding S1100QL with preheating [19,20].

		Technology B: With Preheating	
Preheating Temperature		**Max 200 °C**	
Heat input		8–12 kJ/cm	
Filler materials	Root and filler passes Filler passes	G 89 (according to EN IS 16834)	M21 shielding gas (according to ISO 14175)

Further details regarding the weldability of this steel can also be found in the producer's documentation. The carbon equivalent CET and CEV values calculated by the producer are CET = 0.40 and CEV = 0.70 [19,20]. CET values above 0.35 and CEV values above 0.45 imply bad weldability of the specific steel, indicated that preheating needs to be used. Further details regarding the requirements for preheating based on the calculation of carbon equivalent value are given in [21]. Both values point out that the weldability of this steel is conditional and that precaution and special measures need to be taken when this steel is to be welded.

2.3. Welding Equipment

The authors of this paper decided to weld the prepared plates using a combination of manual welding and a robotic console, both powered by Miller Electrics welding units, allowing for Gas Manual Arc Welding (GMAW)welding to be conducted. The characteristics of the welding unit and the display of the robotic console are displayed in Figure 2.

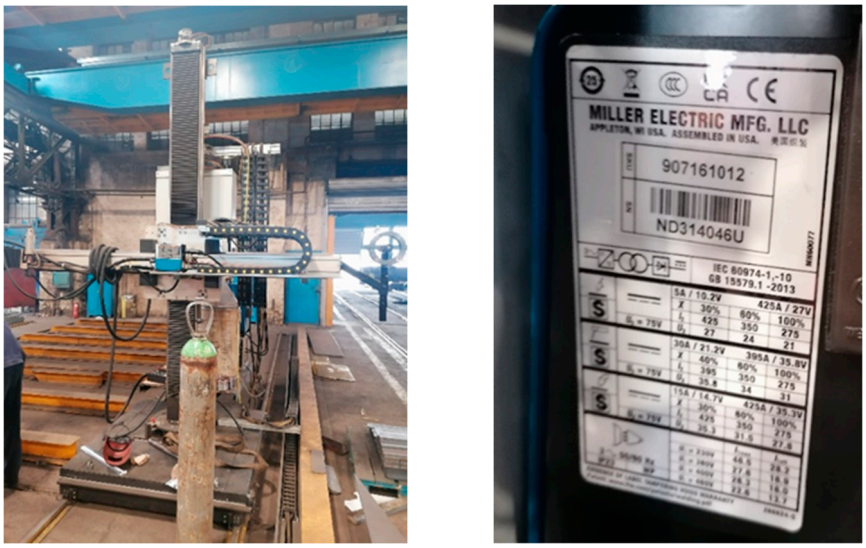

(**a**) (**b**)

Figure 2. The robotic console (**a**) and the characteristics of the GMAW welding unit (**b**).

2.4. Welding Technology A

The prepared plates were joined manually with several tack welds (Figure 3) to form a groove for the weld metal to be deployed. For this technology, according to the steel producer, the root pass was welded using an austenitic stainless-steel filler material and without preheating. In this case, the G 18 8 Mn grade of filler material is recommended, and according to recommendations, the authors chose SI Jesenice's MIG 18/8/6 Si filler material (SI Jesenice, Jesenice and Slovenia), since it fulfills the posed conditions. The chemical composition and mechanical properties, as well as the recommended welding parameters, are displayed in Tables 5–7 [22].

Figure 3. Display tack welded plates.

Table 5. Chemical composition of MIG 18/8/6 filler material.

%C	%Mn	%Si	%Ni	%Cr
0.08	7.0	0.8	9.0	18.5

Table 6. Mechanical properties of MIG 18/8/6 filler material.

$R_{p0.2}$, MPa	R_m, MPa	A_5, %	$KV_{20°C}$, J
min 320	560–660	35	min 40

Table 7. Recommended welding parameters for MIG 18/8/6 filler material.

Welding Current, I, A	Welding Voltage, U, V	Shielding Gas
N/A	N/A	M12 (97.5% Ar + 2.5% $CO_{2)}$

In this technology, preheating the prepared plates is not recommended due to the possible effect of temperature on the properties of the weld metal. According to extensive research experience in earlier work with similar steel grades, the authors chose to slightly preheat the prepared plates before welding the root pass, even though the producer does not recommend this. For this purpose, a liquid petroleum gas (LPG) torch was used to achieve a preheating temperature of 120 °C (Figure 4). The idea was to clean the groove and burn possible impurities found on the beveled edges. The preheating temperature was measured on the plates, 100 mm away from the groove. Heat input is defined by the steel producer, and it ranges from 8 to 12 kJ/cm.

Figure 4. Plate preheating using LPG torch.

After the initial preheating was concluded, the manual welding of the root proceeded. Since the root for this technology was welded manually, after the first pass, the deployed root was ground from both sides and then welded again from both ground sides. This ensured that the welded metal penetrated into the prepared plates. The welding parameters of the root passes are presented in the above table.

According to the steel producer, for further welding of the prepared groove, the G 18 8 Mn filler material was changed to G89 grade. For these welds, a robotic console was used. For this purpose, the authors chose ESAB's ARISTOROD 89. This filler material complies with the producer's recommendations, and it is similar to the base material with slightly lower strength. Chemical composition, mechanical properties, and recommended welding parameters are displayed in Tables 8–10. The scheme of the deployed welds is presented in Figure 5, and the welding parameters for each pass are shown in Table 11 [23].

Table 8. Chemical composition of ARISTOROD 89.

%C	%Mn	%Si	%Ni	%Cr	%Mo
0.081	1.75	0.8	2.22	0.41	0.533

Table 9. Mechanical properties of ARISTOROD 89.

$R_{p0.2}$, %	R_m, %	A	$KV_{-40°C}$, J
920	960	18	55

Table 10. Recommended welding parameters for ARISTOROD 89.

Welding Current, I, A	Welding Voltage, U, V	Shielding Gas
80–280	18–28	M21 (82% Ar + 18% $CO_{2)}$

Table 11. Welding parameters for each pass of the welded joint.

Type of Pass	No. of Pass	I, A	U, V	T_p, °C	v_z, cm/s	q_l, J/cm	Q, l/min	T_i, °C
Root pass	1	175	22	120	0.4	7700	20	120
	2	175	22	120	0.4	7700	20	120
	3	175	22	120	0.4	7700	20	120
Filler pass	4	250	30.1	175	0.6	10,033	20	175
	5	250	30.1	175	0.6	10,033	20	175

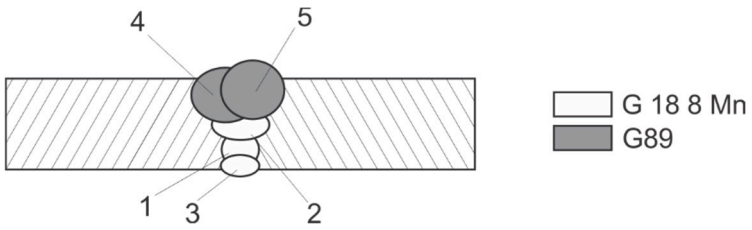

Figure 5. Layer deployment scheme for technology A.

2.5. Welding Technology B

Technology B is the alternative technology recommended by the steel producer. According to the producer's recommendations, this technology included preheating the prepared plates, up to temperatures of 200 °C, and an application of just one filler material, G89 (ESAB, North Bethesda, MD, USA). The recommendations regarding heat input are the same as in the first case, between 8 and 12 kJ/cm. The chemical composition, mechanical properties, and recommended welding parameters of the filler material used were previously displayed. Before welding was initiated, the plates were joined through several small tack welds, the same as displayed in the figure. After tack welds were deployed, preheating of the plates intended for technology B began. Preheating was completed using a liquid petroleum gas (LPG) torch. The selected preheating temperature was 175 °C, and it measured 100 mm from the position of the welded joint. The interpass temperature was also 175 °C. The scheme of deployed welds is displayed in Figure 6, and the parameters used are displayed in Table 12.

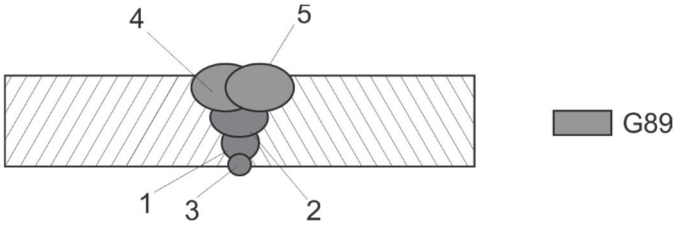

Figure 6. Layer deployment scheme for technology B.

Table 12. Welding parameters for each pass of the welded joint.

Type of Pass	No. of Pass	I, A	U, V	T_p, °C	v_z, cm/s	q_l, J/cm	Q, l/min	T_i, °C
Root pass	1	180	23.6	175	0.4	8496	20	175
Filler pass	2	250	30.1	175	0.6	10,033	20	175
	3	250	30.1	175	0.6	10,033	20	175
	4	250	30.1	175	0.67	8985	20	175
	5	250	30.1	175	0.67	8985	20	175

2.6. Testing

2.6.1. Tensile Testing

The aim of this paper is to display the tensile properties of S1100QL steel (SSAB, Stockholm, Sweeden) and its welded joints at both room and elevated temperatures. Even though this grade of steel is not meant for application at elevated temperatures, this test was conducted as part of common practice among researchers to explore a material's behavior at various conditions. To determine the tensile properties from the base material, cylindrical specimens were machined on CNC lathes. The geometry of the base material specimens and an example of a finished specimen are displayed in Figure 7.

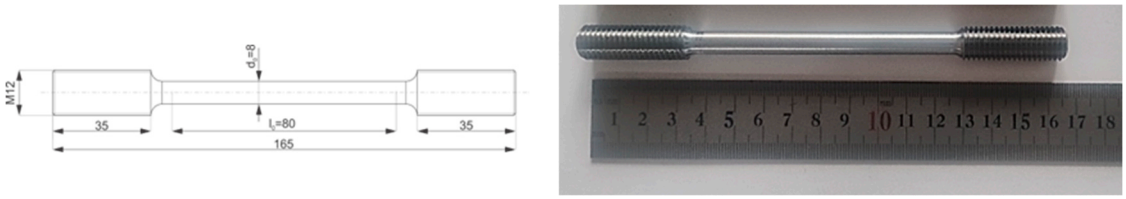

(**a**) (**b**)

Figure 7. (**a**) Geometry of base material specimens; (**b**) machined specimen.

Specimens for tensile testing of welded joints were also CNC machined on a lathe, with similar geometry but different dimensions. In this case, the dimensions were altered to assure the quality of the thread, as its quality is important for connecting specimens with the testing machine. A sketch of the specimen's geometry and a photo of a finished specimen are presented in Figure 8.

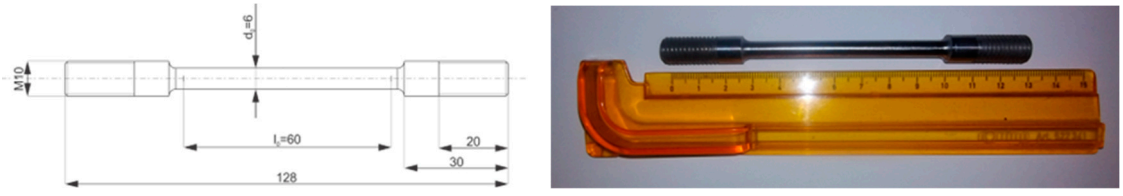

(**a**) (**b**)

Figure 8. (**a**) Sketch of specimen geometry; (**b**) finished specimen.

Tensile testing of all specimens was conducted on the universal tensile testing machine ZWICK ROELL Z/100 (ZWICKROELL GmbH, Ulm, Germany) (Figure 9a). For testing at elevated temperatures, a special MAYTEC, (Singen, Germany) heating chamber was used to allow heating of the specimens (Figure 9b). This heating chamber allows the specimens to be heated at temperatures up to 1000 °C. During the research, the maximum heating temperature did not exceed 700 °C, and the test temperature ranged from room temperature up to 700 °C, for both the base material and the welded joints. The heating chamber contains a special control unit (Figure 9c) that allows the temperature to be controlled and monitored. Once the chamber reached the desired temperature, the specimens were held at that temperature approx. 2 min/1 mm of specimen diameter. The held time ranged from 12 min (for specimens

of welded metal) to 16 min (for base material specimens). The test speed for all specimens was 10 mm/min. For each case of testing, two specimens were broken.

(**a**) (**b**) (**c**)

Figure 9. (**a**) Universal testing machine; (**b**) Maytec heating chamber; (**c**) control unit.

2.6.2. Metallography Testing

Metallography tests were conducted on specimens obtained from both welded technologies. Specimens were carefully prepared (ground and polished), etched (with nitric acid solution and aqua regia), and observed under various magnifications. The aim of this investigation is to connect the obtained microstructures with mechanical properties obtained through tensile testing.

2.6.3. Hardness Measurement

After the metallography tests, the prepared specimens were used to measure hardness in the specific zones of the welded joint. Vickers method (HV 10) was applied. Since the thickness of the welded plates was 12 mm, hardness was measured across the welded joint in two different directions zone near the top and near the root (Figure 10).

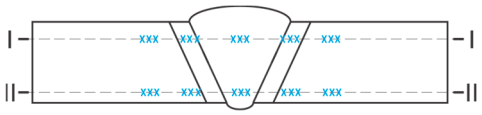

Figure 10. Directions of hardness measurement.

3. Results

3.1. Results of Tensile Testing at Room and Elevated Temperatures

3.1.1. Base Material

The results of tensile testing of the base material at room temperature are displayed in Table 13 below. The yield stress and the ultimate tensile strength are within range of values stated by the steel producer. The elongation values are slightly lower than expected. The stress–strain curve for one of the specimens is displayed in Figure 11, and the broken specimen is displayed in Figure 12.

Table 13. Tensile test results of base material at room temperature.

	$R_{p0.2}$, MPa	R_m, MPa	A, %
1	1140.47	1391.77	7.30
2	1192.86	1395.10	7.73

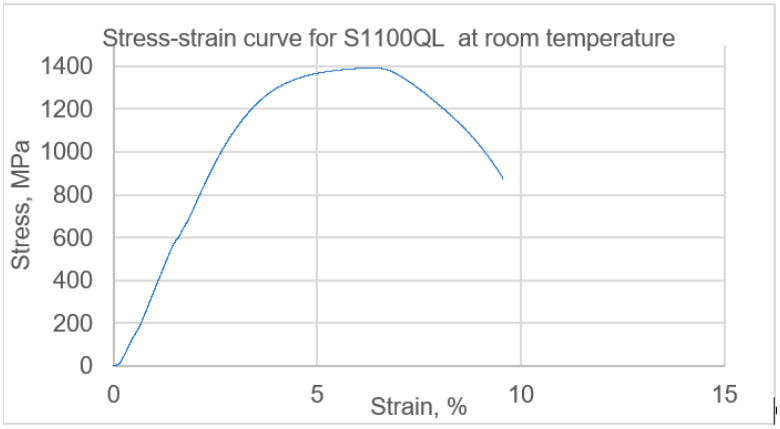

Figure 11. Stress–strain curve for S1100QL at room temperature.

Figure 12. Broken base material specimen after testing at room temperature.

The tensile test results for the base material at elevated temperatures are displayed in Table 14. The results obtained indicate that this steel retains its strength at up to 400 °C. At 500 °C, the strength drastically drops, and elongation begins to rise. This is due to the influence of temperature on the material's plasticity. Examples of the recorded stress–strain curves for all the temperatures tested are displayed in Figure 13. Observing Figure 13, one can notice a sudden drop in strength after 400 °C. Broken specimens are shown in Figure 14.

Table 14. Results of tensile testing of base material at elevated temperatures.

Specimen Number	$R_{p0.2}$, MPa	R_m, MPa	A, %	T, °C
1	1131.99	1379.02	6.86	100
2	1112.99	1374.06	6.77	100
3	1101.49	1370.09	5.35	200
4	1076.79	1375.45	6.05	200
5	1052.00	1416.95	7.85	300
6	1055.72	1436.45	7.43	300
7	1045.55	1373.82	12.07	400
8	1031.73	1334.91	12.35	400
9	876.27	983.98	7.21	500
10	846.36	936.09	7.87	500
11	568.02	627.38	10.51	600
12	575.58	606.96	13.55	600
13	253.95	272.49	30.07	700
14	241.66	259.30	38.8	700

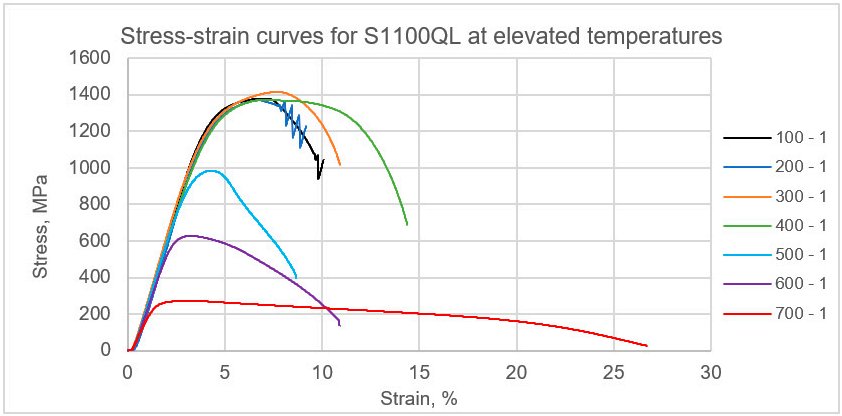

Figure 13. Stress–strain curves for base material at elevated temperatures.

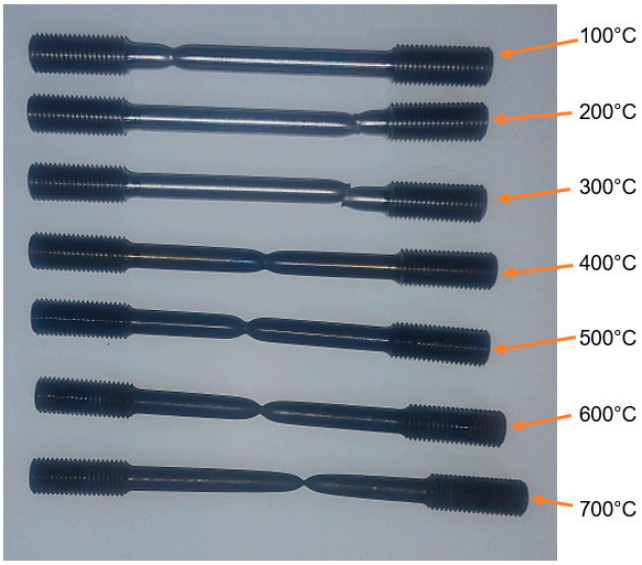

Figure 14. Broken base material specimens after testing at elevated temperatures.

At moderate temperatures (100–400 °C), the tempered martensitic microstructure of S1100QL softens slightly due to the partial relief of internal stresses and the facilitation of dislocation movements. As the temperature rises, thermal activation eases the deformation processes, resulting in increased ductility. Around 500 °C, dynamic strain aging (DSA) typically occurs in quenched and tempered steels like S1100QL. DSA is caused by interactions between diffusing carbon atoms and dislocations, creating localized pinning and subsequent embrittlement. This phenomenon manifests as reduced ductility despite elevated temperatures [24].

In Table 15, the mean values of the parameters and the standard deviation at each considered temperature for the base material are presented. Table 16 contains data regarding the confidence intervals for each considered parameter at the 95% confidence level. These two tables present basic data obtained through statistical analysis. Due to the small number of measurements in one sample, the obtained data lacked precision. The confidence level needed to display the expected value if the experiment was to be repeated under the same conditions. Again, due to the small number of repetitions, this value has a wide range of expected values. This range can be narrower if the number of measurements for each specimen is increased.

Table 15. Mean values of the parameters and the standard deviation at each considered temperature for the base material.

T, °C	$R_{p0.2}$, MPa Mean Value	$R_{p0.2}$, MPa Standard Deviation	R_m, MPa Mean Value	R_m, MPa Standard Deviation	A, % Mean Value	A, % Standard Deviation
RT	1166.67	37.05	1393.44	2.35	7.52	0.30
100	1122.49	13.44	1376.54	3.51	6.82	0.06
200	1089.14	17.47	1372.77	3.79	5.70	0.49
300	1053.86	2.63	1426.70	13.79	7.64	0.30
400	1038.64	9.77	1354.37	27.51	12.21	0.20
500	861.32	21.15	960.04	33.86	7.54	0.47
600	571.80	5.35	617.17	14.44	12.03	2.15
700	247.81	8.69	265.90	9.33	34.44	6.17

Table 16. Mean values of the parameters and the standard deviation at each considered temperature for the base material.

T, °C	Confidence Interval $R_{p0.2}$, MPa		Confidence Interval R_m, MPa		Confidence Interval A, %	
	Lower Bound	Upper Bound	Lower Bound	Upper Bound	Lower Bound	Upper Bound
RT	833.83	1726.27	1372.28	1414.59	4.78	10.25
100	1001.78	1243.20	1345.03	1408.05	6.24	7.39
200	932.22	1246.06	1338.72	1406.82	1.25	10.15
300	1030.23	1077.49	1302.81	1550.59	4.97	10.31
400	950.84	1126.44	1107.17	1601.56	10.43	13.99
500	671.29	1051.34	655.78	1264.29	3.35	11.73
600	523.77	619.83	487.44	746.90	0	31.34
700	169.73	325.88	182.10	349.69	0	89.90

Based on the results presented, the following can be concluded:

Yield Strength, RT to 100 °C: increases from 842.59 MPa to 898.29 MPa (likely due to short-term strain hardening); 100 °C to 200 °C: drops sharply to 842.11 MPa and then fluctuates mildly until 400 °C; 500 °C+: rapid decline (722.57 MPa at 500 °C, 247.74 MPa at 700 °C), indicating thermal softening. Standard Deviation: highest at RT (59.94) and 600 °C (44.14), suggesting variability in material consistency at these temperatures.

Tensile Strength, RT: highest value (1008.48 MPa), decreases with temperature; 100 °C: unexpected drop to 932.87 MPa (SD = 50.01, high variability); 200–400 °C: stabilizes near 890–946 MPa (SD lowers, consistent behavior); 500 °C+: sharp decline (756.88 MPa at 500 °C, 261.84 MPa at 700 °C). Standard Deviation Peaks: at 100 °C (50.01) and 600 °C (38.20).

Elongation, RT to 200 °C: ductility decreases (5.01% → 2.60% → 2.81%), likely due to reduced plasticity; 300–500 °C: recovers slightly (4.66–6.89%), possibly from dynamic recovery mechanisms; 700 °C: surge to 19.43% (SD = 2.57), indicating superplastic behavior or material softening. Standard Deviation Variability: highest at 100–200 °C (~3.0) and 400 °C (3.00). Based on this analysis, 500 °C is marked as a critical threshold when all properties degrade significantly, marking a limit for high-temperature applications.

3.1.2. Technology A

The results of tensile testing of the welded specimens at room temperature are displayed in Table 17. The results obtained are within expectations, with slightly lower elongation, compared to the base material. This is a consequence of the heat input during welding, which alters the microstructure of steel. The results obtained at room temperature are displayed in the table below. The stress–strain curve for one of the specimens is displayed in Figure 15. An example of the broken specimen is given in Figure 16.

Table 17. Results of tensile testing specimens from technology A.

Specimen Number	$R_{p0.2}$, MPa	R_m, MPa	A, %
1	884.97	1016.28	4.23
2	800.20	1000.67	5.79

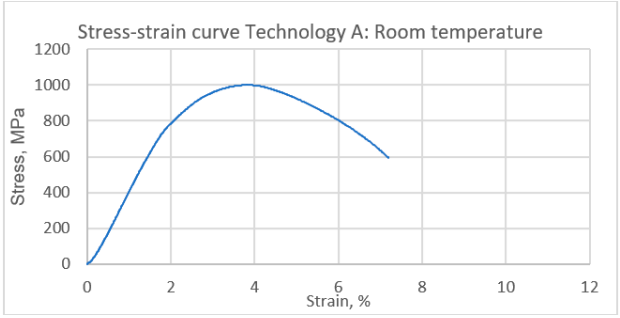

Figure 15. Stress–strain curve at room temperature of the specimen welded with technology A.

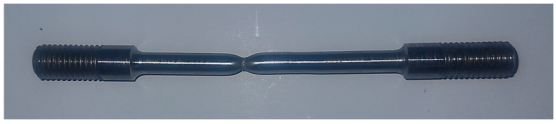

Figure 16. Broken technology A specimen after testing at room temperature.

The tensile tests results for welded specimens at elevated temperatures are displayed in Table 18, and the recorded stress–strain curves are displayed in Figure 17 below. From the results obtained and the showcased stress–strain curves, it can be noticed that with increasing temperature the strength moderately drops. At temperatures up to 400 °C, the strength is lower than at room temperature, but it is not dropping. At 500 °C and 600 °C, the strength is slightly degrading, while elongation rises. Finally, at 700 °C, the strength drops drastically, and the elongation values exceed 20%. Display of broken specimens is given on the Figure 18.

Table 18. Recorded results for specimens from technology A at elevated temperatures.

Specimen Number	$R_{p0.2}$, MPa	R_m, MPa	A, %	T, °C
1	915.69	968.23	4.71	100
2	880.88	897.5	0.48	100
3	858.69	894.07	0.64	200
4	825.52	887.71	4.97	200
5	852.13	931.32	5.28	300
6	883.52	958.46	5.01	300
7	816.72	936.12	2.54	400
8	875.85	956.8	6.78	400
9	725.2	752.4	6.43	500
10	719.94	761.36	7.35	500
11	570.31	582.9	7.27	600
12	507.88	528.87	1.95	600
13	255.57	270.12	17.61	700
14	239.91	253.56	21.24	700

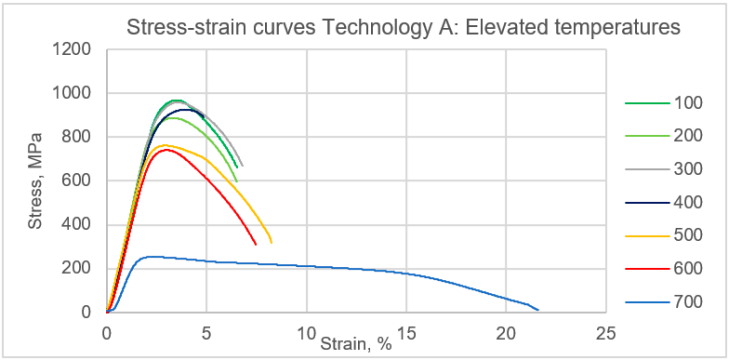

Figure 17. Stress–strain curves for technology A specimens at elevated temperatures.

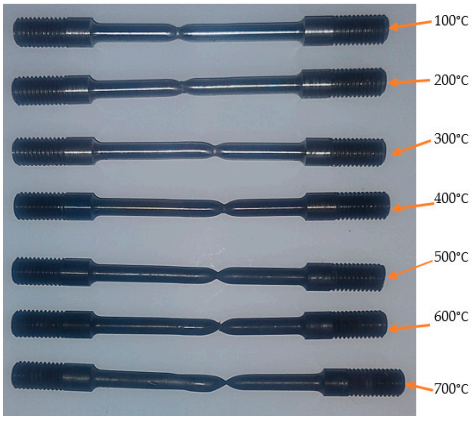

Figure 18. Broken technology A specimens after testing at elevated temperatures.

In Table 19, the mean values of the parameters and the standard deviation at each considered temperature for the base material are presented. Table 20 contains data regarding the confidence intervals for each considered parameter at the 95% confidence level. Here, it needs to be highlighted that determination of the mean value, standard deviation, and confidence interval was based on a single sample based on two measurements (two repetitions of a tensile test); therefore, the data obtained cannot be taken into consideration with great precision.

Table 19. Mean values of the parameters and the standard deviation at each considered temperature for Technology A.

T, °C	$R_{p0.2}$, MPa Mean Value	$R_{p0.2}$, MPa Standard Deviation	R_m, MPa Mean Value	R_m, MPa Standard Deviation	A, % Mean Value	A, % Standard Deviation
RT	842.59	59.94	1008.48	11.04	5.01	1.10
100	898.29	24.61	932.87	50.01	2.60	2.99
200	842.11	23.45	890.89	4.50	2.81	3.06
300	867.83	22.20	944.89	19.19	5.15	0.19
400	846.29	41.81	946.46	14.62	4.66	3.00
500	722.57	3.72	756.88	6.34	6.89	0.65
600	539.10	44.14	555.89	38.20	4.61	3.76
700	247.74	11.07	261.84	11.71	19.43	2.57

Table 20. Mean values of the parameters and the standard deviation at each considered temperature for the base material.

T, °C	Confidence Interval $R_{p0.2}$, MPa		Confidence Interval R_m, MPa		Confidence Interval A, %	
	Lower Bound	Upper Bound	Lower Bound	Upper Bound	Lower Bound	Upper Bound
RT	304.03	1381.14	909.30	1107.65	0	14.92
100	677.13	1119.44	483.51	1382.22	0	29.47
200	631.37	1052.84	850.48	931.30	0	30.31
300	668.40	1067.25	772.47	1117.31	0	6.86
400	470.63	1221.94	815.08	1077.84	0	31.60
500	689.15	755.99	699.96	813.80	1.05	12.73
600	142.47	935.72	212.63	899.14	0	38.41
700	148.25	347.23	156.63	367.05	0	42.49

Based on the presented results, the following can be concluded for welding technology A (Table 18):

Yield Strength, RT to 100 °C: peaks at 898.29 MPa (SD = 24.61); 500 °C+: sharp decline to 247.74 MPa at 700 °C.

Tensile Strength, RT: 1008.48 MPa (SD = 11.04, highly consistent); 100 °C: sudden drop to 932.87 MPa (SD = 50.01); 700 °C: falls to 261.84 MPa.

Elongation, RT: 5.01% (SD = 1.10); 700 °C: surges to 19.43% (SD = 2.57, ductile at high temps).

Technology A outperforms the base material in precision (lower SDs, narrower CIs) and predictability (consistent trends across temperatures). The base material is unreliable due to extreme CIs (e.g., Rm at 100 °C ranges from 483.51 to 1382.22 MPa), risk of brittleness (0% elongation lower bounds), and critical temperature (500 °C+). Both materials weaken, but technology A degrades more gradually.

3.1.3. Technology B

The tensile test results obtained show that at room temperature the yield stress and ultimate tensile strength are slightly lower compared with the results obtained for Technology A's welded joint. Elongation values are also lower than the results obtained with technology A. The results are displayed in Table 21, and one example of a stress–strain curve is displayed in Figure 19, and a broken specimen is shown in Figure 20.

Table 21. Stress–strain curves for specimens from technology B.

Specimen Number	$R_{p0.2}$, MPa	R_m, MPa	A, %
1	785.36	957.99	6.42
2	770.32	942.52	6.09

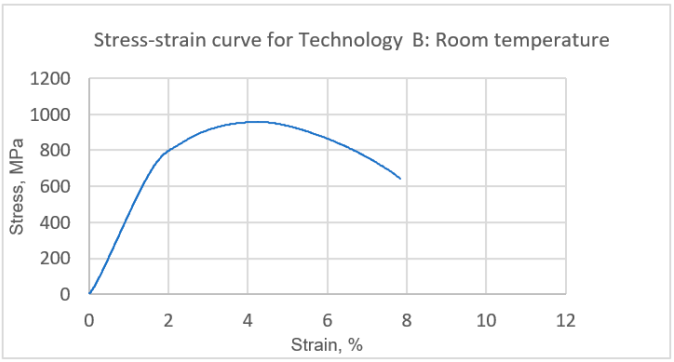

Figure 19. Stress–strain curve for technology B at room temperature.

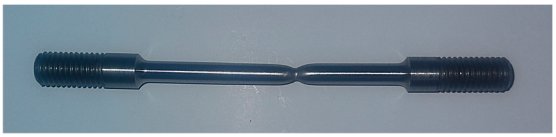

Figure 20. Broken technology B specimen after testing at room temperature.

The results displayed (Table 22) show that the yield stress and ultimate tensile strength values are similar up to 400 °C. At temperatures higher than that, the strength begins to slowly degrade, which confirms the results of tests at 500 °C, 600 °C, and 700 °C. As the test temperature increases, elongation values rise as well, reaching their maximum values at 700 °C (Figure 21). The specimens after experimental testing are displayed in Figure 22.

Table 22. Results of tensile testing of technology B specimens at elevated temperatures.

	$R_{p0.2}$, MPa	R_m, MPa	A, %	T, °C
1	804.06	852.77	2.07	100
2	853.51	907.97	3.77	100
3	839.35	890.94	5.48	200
4	802.99	864.89	5.93	200
5	817.02	881.62	5.58	300
6	826.54	894.79	5.55	300
7	813.49	916.18	4.96	400
8	808.82	923.54	7.21	400
9	693.82	764.70	6.40	500
10	709.17	762.53	6.65	500
11	551.01	567.03	7.21	600
12	539.35	558.16	7.44	600
13	234.40	245.44	20.79	700
14	248.54	261.48	18.01	700

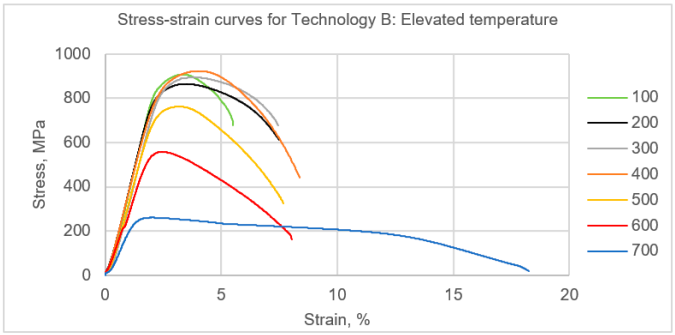

Figure 21. Stress–strain curves for specimens from technology B at elevated temperatures.

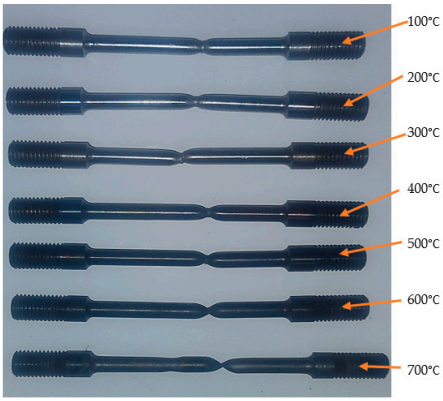

Figure 22. Specimens from technology B after testing at elevated temperatures.

In Table 23, the mean values of the parameters and the standard deviation at each considered temperature for the base material are presented. Table 24 contains data regarding the confidence intervals for each considered parameter at the 95% confidence level. As in the previous case, due to a lack of repetitions, statistical data need to be carefully assessed.

Table 23. Mean values of the parameters and the standard deviation at each considered temperature for technology A.

T, °C	$R_{p0.2}$, MPa Mean Value	$R_{p0.2}$, MPa Standard Deviation	R_m, MPa Mean Value	R_m, MPa Standard Deviation	A, % Mean Value	A, % Standard Deviation
RT	777.84	10.63	950.26	10.94	6.26	0.23
100	828.79	34.97	880.37	39.03	2.92	1.20
200	821.17	25.71	877.92	18.42	5.71	0.32
300	821.78	6.73	888.21	9.31	5.57	0.02
400	811.16	3.30	919.86	5.20	6.09	1.59
500	701.50	10.85	763.62	1.53	6.53	0.18
600	545.18	8.24	562.60	6.27	7.33	0.16
700	241.47	10.00	253.46	11.34	19.40	1.97

Table 24. Mean values of the parameters and the standard deviation at each considered temperature for the base material.

T, °C	Confidence Interval, $R_{p0.2}$, MPa		Confidence Interval, R_m, MPa		Confidence Interval, A, %	
	Lower Bound	Upper Bound	Lower Bound	Upper Bound	Lower Bound	Upper Bound
RT	682.29	873.39	851.97	1048.54	4.16	8.35
100	514.62	1142.95	529.68	1231.06	0	13.72
200	590.17	1052.17	712.42	1043.41	2.85	8.56
300	761.30	882.26	804.53	971.88	5.37	5.76
400	781.49	840.82	873.10	966.62	0	20.38
500	603.97	799.02	749.83	777.40	4.94	8.11
600	471.10	619.26	506.24	618.95	5.86	8.79
700	151.64	331.30	151.56	355.36	1.74	37.06

Based on the results presented, the following can be concluded for welding technology B (Table 22):

Yield Strength, RT to 100 °C: increases from 777.84 MPa → 828.79 MPa (likely due to initial strain hardening); 100 °C to 400 °C: gradual decline (828.79 → 811.16 MPa) but remains stable (SD ≤ 34.97); 500 °C+: significant drop (701.50 MPa at 500 °C, 241.47 MPa at 700 °C), indicating thermal softening.

Standard Deviation: lowest at 400 °C (3.30) and 300 °C (6.73) (high consistency), highest at 100 °C (34.97) (possible experimental variability).

Conclusion: best performance at 100–400 °C (high strength, low variability), avoid > 500 °C (rapid strength loss).

Tensile Strength, RT: 950.26 MPa (SD = 10.94, highly consistent); 100 °C: drops to 880.37 MPa (SD = 39.03, higher variability); 200–400 °C: stabilizes (877.92–919.86 MPa) with improving SDs (as low as 5.20 at 400 °C); 500 °C+: sharp decline (763.62 MPa → 253.46 MPa).

Standard Deviation Trends: most stable at 500 °C (SD = 1.53) and 600 °C (6.27).

Conclusion: optimal consistency at 300–600 °C (low SDs); critical threshold at 500 °C (strength degradation begins).

Elongation, RT: 6.26% (SD = 0.23, very consistent); 100 °C: lowest ductility (2.92%, SD = 1.20); 200–600 °C: recovers (5.57–7.33%) with minimal SDs (≤1.59); 700 °C: surges to 19.40% (SD = 1.97), suggesting superplasticity.

Conclusion: ductility drops at 100 °C (may indicate embrittlement); excellent high-temperature ductility (>600 °C).

When compared to technology A, technology B shows higher consistency, lower standard deviation in $R_{p0.2}$ (e.g., 3.30 at 400 °C vs. 41.81 in Table 18), more stable R_m (SDs ≤ 39.03 vs. 50.01 in Table 18) and improved ductility, and higher elongation at RT (6.26% vs. 5.01%) and 700 °C (19.40% vs. 19.43%).

3.2. Metallography Investigation

Samples for metallography tests were cut from plates welded according to previously described technologies. Metallography samples were carefully ground, polished, and finally etched so that they could be observed under various magnifications. For technology A, etching was completed using aqua regia, since the root pass was performed using stainless steel filler material. A sample from welded plate B was etched using nitric acid solution.

3.2.1. Technology A

The macro view of the cross-section of the welded joint (Figure 23) clearly shows a multi-pass GMAW weld, with a fully formed root and filler welds. The root of the weld is symmetrical, with even distribution of heat-affected zones (HAZs) on both sides. In the lower part of the joint, the root is made with austenitic filler material G 18 8 Mn, which is characterized by a slightly lighter structure after etching, which indicates a different chemical composition compared to the rest of the weld.

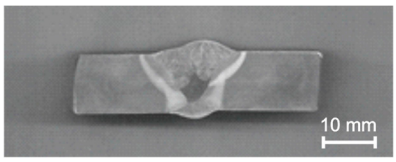

Figure 23. Macroscopic view of the plate's cross-section.

In the middle and upper parts of the bead, several passes with the G89 filler material are observed. Weld layers overlap well without visible porosity, inclusions, or discontinuities. The fusion lines between the weld and the base material are clearly defined, continuous, and without the appearance of macrocracks. The heat-affected zone (HAZ) on both sides has a symmetrical shape, with a smooth transition into the base material, without signs of overheating or disproportionate expansion.

The complete joint is characterized by excellent metallurgical connection and uniformity, as well as good penetration and geometric characteristics, which indicates well-controlled welding parameters—heat input, preheating, and interpass temperatures.

The microstructure of both samples was observed with 200× magnification. The results obtained for welding technology A are displayed in Figure 24.

In Figure 24a, the base material shows a homogenous, fine-grained martensitic structure without any segregations, carbides, or microcracks. The structure present shows the results of the complex heat treatment of QL steel grades, which consists in quenching and low tempering. This combination of heat treatment allows great strength to be achieved while retaining decent toughness. The structure presented is to be expected in UHSS steel

grades [25–27]. The microstructure of welded zones is very important from the aspect of resistance to crack appearance in HSS, which is proven in [28,29].

Figure 24b clearly demonstrates alterations in the microstructure of HAZ compared to the structure of the base material. These alterations occur due to fast cooling of the material after welding. The structure obtained is heterogenous, and a few characteristic zones can be observed. The upper zone on the figure shows a coarser structure, with the brighter and darker zones highlighted. The structure in the lower zone is similar to the structure in the upper zone. The structure of HAZ obtained probably results from the higher strength of the HAZ and lower toughness.

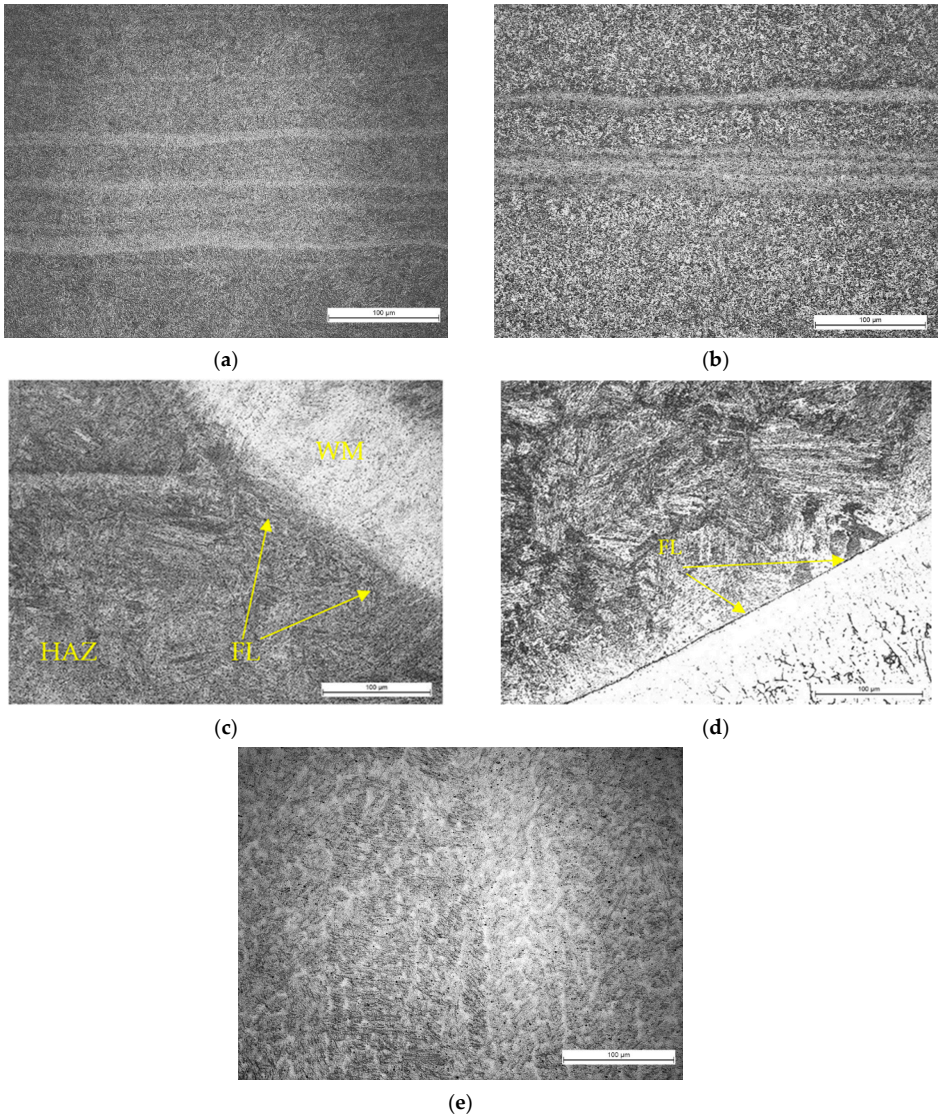

Figure 24. Microscopic view of the structures obtained in the plate welded with technology A under 200× magnification: (**a**) base material; (**b**) Heat-affected zone; (**c**) fusion line near the top surface; (**d**) fusion line near the root; (**e**) weld metal.

The microscopic image given in Figure 24c is of the fusion zone and clearly shows the transition between the weld metal (right) and the heat-affected zone (HAZ) (left). The fusion line is clear, continuous, and without any defects, which indicates a good bond.

A clearly defined fusion line can be observed near the root of the weld zone (Figure 24d), between the austenitic filler material (G 18 8 Mn) and the base steel S1100QL. The transition between the two structures is smooth and defect-free, indicating good metallurgical bonding. The use of the austenitic filler material in the root is justified by its

high toughness and stress absorption capacity, which is especially important in joints with high-strength base steels such as S1100QL.

The microstructure of the weld metal (Figure 24e), obtained by using the high-strength G89 filler material, shows a complex structure. This weld metal in combination with the austenitic root represents a well-balanced weld in terms of mechanical properties and toughness.

In Figure 25, a microscopic display of the same weld sample under greater magnification (500×) is given. In Figure 25a, the microstructure of the base metal is given. The given structure can be described as tempered martensite with precipitated carbides. The given structure is to be expected in this grade of steel, since it provides great balance between strength and toughness. Precipitated carbides are observed, in smaller sections, formed as a consequence of the tempering process.

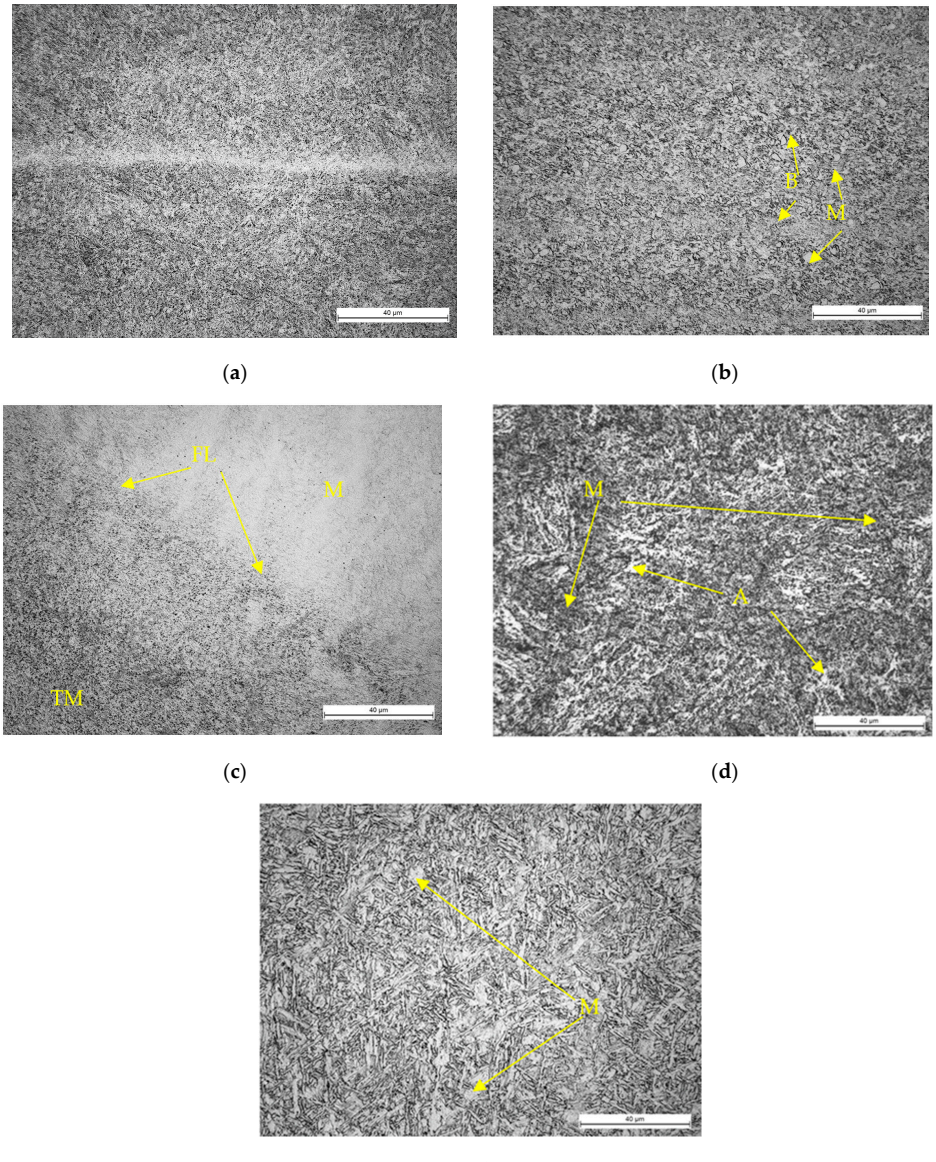

Figure 25. Microscopic view of the structures obtained in the plate welded with technology A under 500× magnification: (**a**) base material; (**b**) HAZ; (**c**) fusion line near the top surface; (**d**) fusion line near the root; (**e**) weld metal.

Figure 25b provides an image of the microstructure in the HAZ of the welded joint. Again, structure alteration compared to the base material is clearly observed, and it was

caused by heat input during the welding process. Tempered martensite with precipitated carbides and a small addition of bainite is observed in the given figure.

In the micrograph displayed in Figure 25c, the fusion line between zones is observed. On the left, darker side, HAZ is shown, while on the right, brighter side the structure of the weld metal is displayed. On the left side, fine-grained tempered martensite (TM) can be observed, formed as consequence of the welding thermal cycle, while on the right side a coarse martensite structure is seen, created as a consequence of fast cooling and solidification.

Figure 25d represents the fusion line between the weld metal and the base material but in the lower portion of the welded joint where austenitic filler material was used. On the graph, a complex structure can be observed that was formed as a consequence of joining two different steel structures. The lighter zones show the austenite grains (A), while the darker zones imply the presence of martensite (M) with precipitated carbides.

In Figure 25e, the microstructure of the weld metal is displayed. In the figure, coarse lath-like martensite with carbide precipitates can be clearly observed. Due to fast cooling and solidification, a coarse lath shape is obtained, worsening the mechanical properties of the joint.

3.2.2. Technology B

A macrostructure view of a cross-section of a Technology A welded joint made of S1100QL steel with a thickness of 12 mm is presented in Figure 26. The joint was made in five passes, where the root of the weld was formed with a lower heat input (8 kJ/cm), while the other passes were realized with an energy of 10 kJ/cm, which achieved good filling and bonding of the layers.

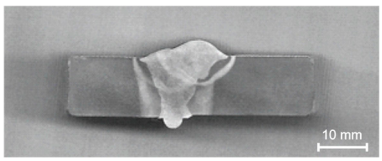

Figure 26. Macrostructure view of technology B welded joint cross-section.

A regular and symmetrical shape of the seam was observed, with a slight convexity on the surface. The root of the seam is properly formed, with no observed defects such as fusion failures, incomplete parts, or porosities. The contour of the weld shows clearly defined thermal zones; darker zones along the weld border indicate the heat-affected zone (HAZ), which is a consequence of the thermal cycle due to welding. Those zones are most pronounced along the face and sides of the seam, where heat accumulated during multi-layer welding.

The transitions between weld passes are noticeable and show a proper multi-layered technique. The thermal etch color clearly differentiates the individual weld layers. There are no visible microstructural discontinuities or defects, which confirms a good quality applied technological process.

The dimensions of the HAZ and the shape of the welded bead are in accordance with the expectations for high-alloy steel welded without PWHT, with controlled preheating and interpass temperature.

In Figure 27, microstructures of the welded joint of technology B under 200× magnification are presented. The structure of the base material is similar to the structure obtained in the first case, so the same description regarding tempered martensite also fits here (Figure 27a).

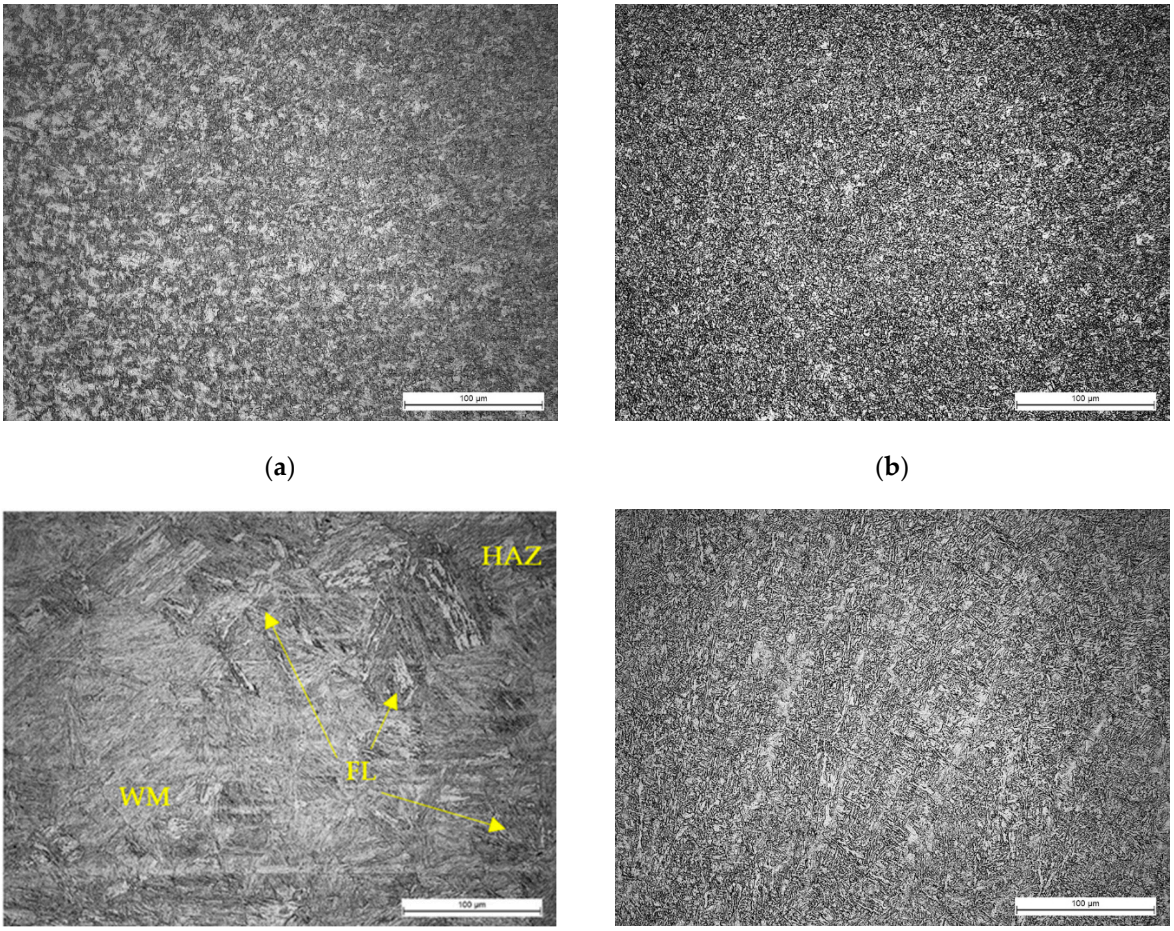

(**a**) (**b**)

(**c**) (**d**)

Figure 27. Microscopic view of the structures obtained in the plate welded with technology B under 200× magnification: (**a**) base material; (**b**) HAZ; (**c**) fusion line; (**d**) weld metal.

The microstructure shown in Figure 27b shows the microstructure of the heat-affected zone (HAZ), which was formed as a result of welding S1100QL steel without subsequent heat treatment. Pronounced grain growth was observed relative to the base material, which is characteristic of the coarse-grained zone of the HAZ (CGHAZ). The structure of this zone indicates increased hardness but also increased brittleness, which can negatively affect the fracture resistance of the welded joint under dynamic loading conditions.

Figure 27c shows the microstructure in the fusion zone of a welded joint of S1100QL steel. The left side of the image represents the weld metal, while the right side is the heat-affected zone (HAZ). The image was taken at a magnification of 200×. The heat-affected zone (HAZ) on the right side of the image shows typical characteristics of a coarse-grained HAZ (GHAZ). The boundary between the weld and the HAZ is sharply defined, with an abrupt transition in morphology and grain orientation. This micrograph is significant because it clearly illustrates the microstructural contrast between the weld metal and the heat-affected zone of the base material. Such changes in structure represent critical zones in terms of mechanical integrity, as they are potential sites of stress concentration and fracture initiation during service.

Figure 27d shows the microstructure of the weld metal obtained by welding S1100QL steel with G89 wire (Aristorod 89). A homogeneous structure without observed segregations confirms that the welding was carried out with good heat control and the correct cooling regime.

Figure 28 presents microstructures in the characteristic zones of welded joints under 500× magnification.

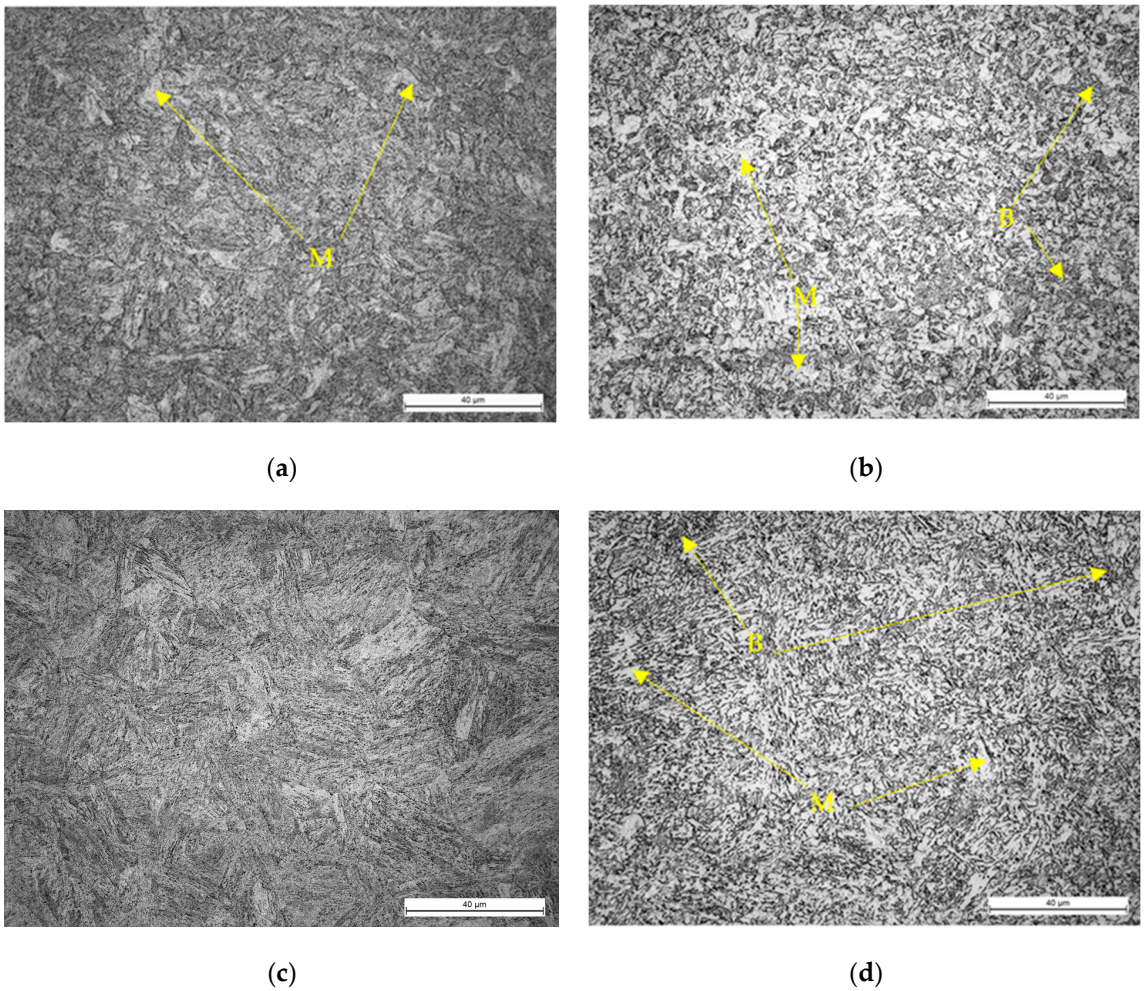

(**a**) (**b**)

(**c**) (**d**)

Figure 28. Microscopic view of structures obtained in plate welded with technology B under 500× magnification: (**a**) base material; (**b**) HAZ; (**c**) fusion line; (**d**) weld metal.

Figure 28a presents the structure of the base material. The structure displayed can be described as fine needle-like tempered martensite with carbide precipitations along the grain boundaries. A fine needle shape implies that the cooling speed of the joint was controlled compared to the structures in the previous technology.

In Figure 28b, the structure of the HAZ is displayed. Due to welding temperature cycle, alterations in the structures were introduced. On the presented micrograph, the structure of the tempered martensite with precipitated carbides and the addition of a bainite structure can be observed. This implies that slightly better mechanical properties are provided by this technology compared to the first. The structure is homogenous without disruptions.

The micrograph in Figure 28c presents the structure of the fusion line between the HAZ and weld metal. Due to longer exposure to high temperatures and faster cooling after welding, a coarser martensitic structure is observed.

The structure presented in Figure 28d was observed in the weld metal. A coarse martensite structure with a small portion of bainite islands is observed. Compared to the first structure, in this case, the grains are finer; thus, better properties are expected in this case.

3.3. Hardness Measurement

3.3.1. Technology A

The results of the hardness measurement are presented in Table 25 and in Figures 29 and 30. Figure 29 displays the hardness of the upper portion of the welded joint, near the top surface. The results obtained of hardness coincide with the microstructures obtained in the welded joint. Here, it needs to be emphasized that the hardness of the weld metal in the root is drastically lower than in the upper zone. This is due to the application of an austenitic filler material with lower hardness. In the upper portion of the weld metal, a martensitic structure is obtained; thus, greater hardness values were measured.

Table 25. Hardness distribution in the welded joint of technology A.

Technology A															
Direction/Zone	**BM**			**HAZ**		**FL**		**WM**		**FL**		**HAZ**		**BM**	
No.	**1**	**2**	**3**	**1**	**2**	**1**	**1**	**2**	**3**	**1**	**1**	**2**	**1**	**2**	**3**
I-I	373	370	370	325	322	319	425	420	425	327	330	325	394	390	397
II-II	387	383	373	311	309	309	220	228	232	336	311	306	387	390	390

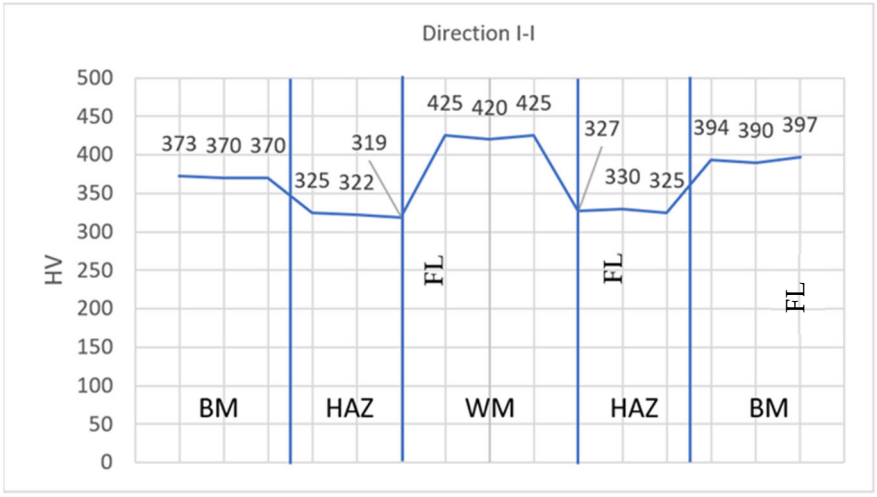

Figure 29. Hardness distribution throughout direction I-I on the technology A welded joint.

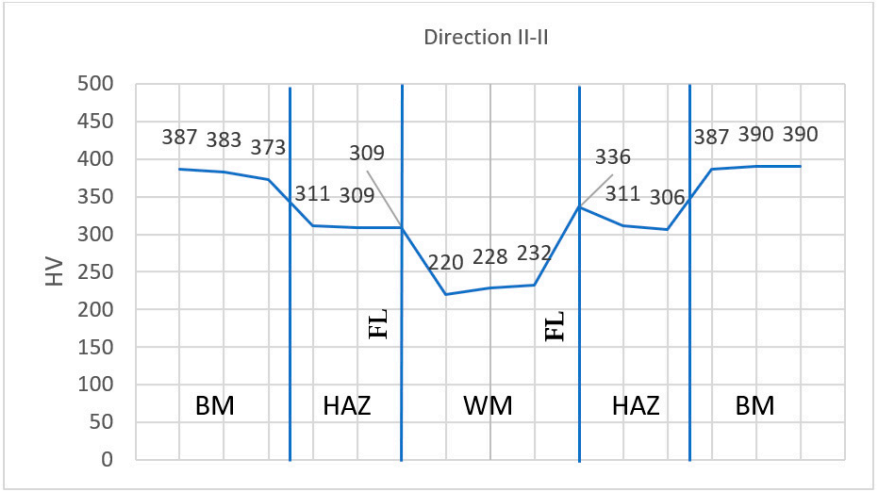

Figure 30. Hardness distribution throughout direction II-II on the technology A welded joint.

3.3.2. Technology B

The results of the hardness measurement are presented in Table 26 and in Figures 31 and 32. Figure 31 displays the hardness of the upper portion of the welded joint, near the top surface.

In this technology, only one filler material was used, which is similar to the base material, and the hardness in almost all zones in both directions has similar values. This implies that the structure of whole weld is homogenous.

Table 26. Hardness distribution in welded joint of technology B.

Technology B															
Direction/Zone No.	**BM**			**HAZ**		**FL**	**WM**			**FL**	**HAZ**		**BM**		
	1	**2**	**3**	**1**	**2**	**1**	**1**	**2**	**3**	**1**	**1**	**2**	**1**	**2**	**3**
I-I	397	397	394	325	333	383	306	311	325	380	372	342	387	405	409
II-II	394	387	387	309	303	318	310	310	302	311	297	314	403	405	417

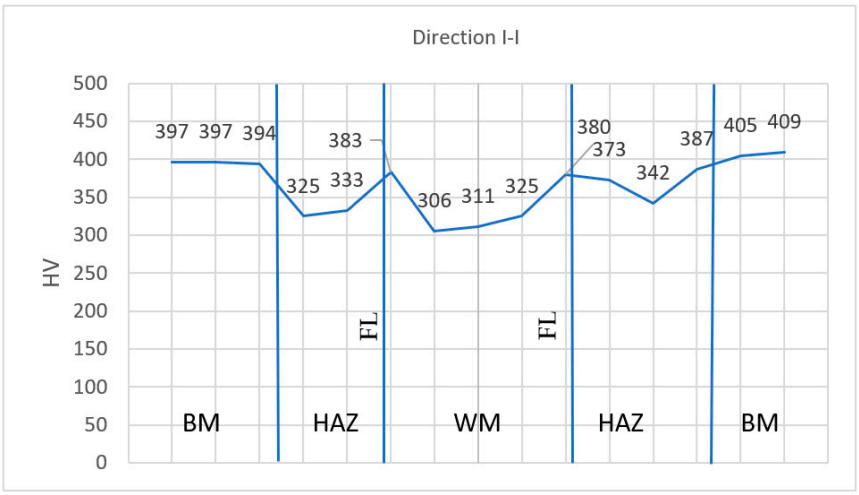

Figure 31. Hardness distribution throughout direction I-I on the technology B welded joint.

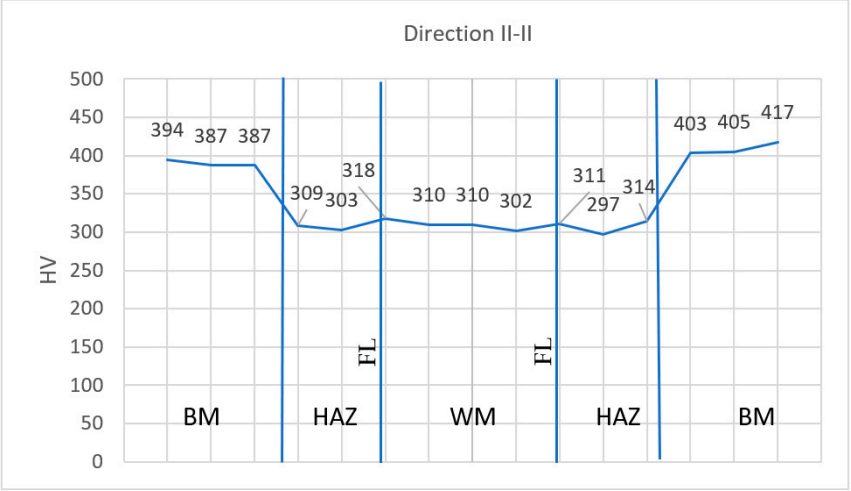

Figure 32. Hardness distribution throughout direction II-II on the Technology B welded joint.

4. Discussion

Tensile testing results for base material S1100QL show that this steel retains high strength up to 400 °C. Up to this temperature, values of the yield strength and ultimate tensile strength show very slight degradation. At temperatures over 400 °C, strength degradation is significant while ductility increases. At 500 °C, a critical point is observed since the strength suddenly drops at that temperature. The results are in accordance with previous results where the behaviors of similar steels at elevated temperatures, such as S690QL and H11, were studied. Degradation of strength was also observed in those studies between 450 °C and 550 °C.

Regarding welded joints, one can notice that the welding technology had a significant impact on the strength and other mechanical characteristics of the welded joints. Technology A, where two filler materials were combined, an austenitic filler material for the root and a steel wire for the other passes, shows higher yield strength and tensile strength compared to technology B. However, elongation values are lower for technology A. This is probably due to heterogeneity of the microstructure and the sharp transition between zones with different materials in the welded joint. This is supported by significant differences in the hardness of the root (austenitic weld metal) and the rest of the weld (martensitic–bainite structure). This can cause localized stress and initiate cracks when subjected to load.

Technology B uses only one filler material, G89 (ARISTO ROD 89), for the whole welded joint. This results in a joint with a more homogeneous microstructure throughout the whole welded joint. The results of the hardness measurement confirm this, since the values obtained are almost uniform along the joint. Even though Technology B has slightly lower strength values compared to technology A, a homogenous structure can lead to better reliability of the welded joints, especially under variable load conditions.

Throughout the analysis, microstructure differences in weld behavior have been confirmed. The presence of different structures in technology A (martensite, bainite, austenite), especially in the weld metal and the HAZ, indicate that the material was subjected to a complex thermal cycle and that there is possible stress accumulation. On the other side, in technology B, a more uniform microstructure with a well-formed fusion line and pronounced lath martensite throughout the weld was observed, in contrast to the structures obtained in technology A. This is expected for UHSS steels welded without subsequent heat treatment.

Analyzing the behavior of welded joints at elevated temperatures, one can notice that up to 400 °C, the mechanical properties and primary strength do not degrade significantly. This potentially sets a limit for the safe operation of structures made of S1100QL steel and its welded joints up to that temperature. Between 500 °C and 600 °C, an even greater decrease in the strength of both the base material and the welded joints occurs. At 700 °C, the decrease in strength is even higher, but an increase in the material's ductility is observed. This ductility increase is directly connected to the increased dislocation mobility and relaxation of the martensite structure under the influence of temperature.

The results displayed show that for structures exposed to elevated temperatures, it is advised to produce that structure using welding technology B due to the homogenous structure and stable mechanical properties. Technology A offers a higher level of strength, but at the cost of heterogenous structure and the possible presence of local weak points.

5. Conclusions

In this article, the mechanical properties of UHSS S1100QL and its welded joints at room and elevated temperatures were experimentally tested and analyzed. Based on the experimental results, the following conclusions can be drawn:

- S1100QL holds high strength up to 400 °C. Above this temperature, at 500 °C or above, there is a sudden decrease in the yield stress and ultimate tensile strength. Vice versa, elongation values increase due to the increase in material plasticity. The critical temperature for the use of this steel without significant strength loss is 400 °C.
- The welded specimens indicated that the mechanical properties of the welded joint depend on the applied welding technology. Technology A uses a combination of austenitic and steel filler material, resulting in higher joint strength but lower ductility and structural heterogeneity. These potentially affect the concentration of stress and the presence of local damage.

- Technology B only uses G89 (ARISTOROD 89) filler material and provides welded joints with a homogenous microstructure. This is confirmed throughout the hardness measurement along the entire joint. Even though the strength of the joints is slightly lower compared to technology A, a homogeneous structure contributes to more stable behavior under variable load conditions.
- Analyses of the microstructure confirm the presence of a martensite and bainite structure in the weld metals and heat-affected zones. Depending on the weld technology, differences in phase distribution and grain size are observed. Technology B showed a more uniform microstructure and better integration of the weld zones and the base material.
- For future structures operating at elevated temperatures, application of technology B is recommended, since it provides better reliability and homogeneity of the structure, while technology A is more suitable when high strength is the priority. In this case, careful analysis of loads and operating conditions needs to be conducted.

This study allows for a better understanding of the behavior of S1100QL steel and its welded joints at high temperatures. This is of great importance for the safe design of reliable structures made of this advanced steel.

Author Contributions: Conceptualization, D.I. and D.A.; methodology, M.D.; software, J.M.; validation, N.I., L.R. and A.I.; investigation, N.I. and D.I.; resources, D.I., D.A. and D.I.; writing—original draft preparation, D.I.; writing—review and editing, D.A.; visualization, M.D.; supervision, D.A.; funding acquisition, D.A. All authors have read and agreed to the published version of the manuscript.

Funding: This research was partially supported by the Ministry of Science and Faculty of Engineering, University in Kragujevac (contract nos. 01–1/750–78; 01–1/750–33, 01–1/580–45).

Institutional Review Board Statement: Not applicable.

Informed Consent Statement: Not applicable.

Data Availability Statement: Data are contained within this article.

Acknowledgments: The authors wish to thank company SSAB SWEDISH STEEL d.o.o. for their donation of steel plates used for sample preparation, as well as to GOŠA FOM a.d. Smederevska Palanka, Serbia for providing extensive technical support for the welding of S1100QL. The authors want to express great gratitude to the company PROMEK d.o.o., Velika Plana, Serbia for providing help with specimen preparation.

Conflicts of Interest: The authors declare no conflicts of interest.

References

1. Cobb, H.M. *The History of Stainless Steel*; ASM International Materials Park: Novelty, OH, USA, 2010.
2. Pang, S.; Wang, W. Fire resistance design of high strength steel H-section columns under axial compression. *J. Constr. Steel Res.* **2025**, *227*, 109414. [CrossRef]
3. Qiang, X.; Jiang, X.; Bijlaard, F.S.K.; Kolstein, H. Mechanical properties and design recommendations of very high strength steel S960 in fire. *Eng. Struct.* **2016**, *112*, 60–70. [CrossRef]
4. Neuenschwander, M.; Scandella, C.; Knobloch, M.; Fontana, M. Modeling elevated-temperature mechanical behavior of high and ultra-high strength steels in structural fire design. *Mater. Des.* **2017**, *136*, 81–102. [CrossRef]
5. Lassi, K.; Kangaspuoskari, M.; Niskanen, J. Ultra high-strength steels at elevated temperatures. *J. Constr. Steel Res.* **2021**, *183*, 106739. [CrossRef]
6. Lazić, V.; Aleksandrović, S.; Arsić, D.; Sedmak, A.; Ilić, A.; Đorđević, M.; Ivanović, L. The influence of temperature on mechanical properties of the base material and welded joint made of steel S690QL. *Metallurgy* **2016**, *55*, 213–216.
7. Arsić, D.; Djordjević, M.; Zivković, J.; Sedmak, A.; Aleksandrović, S.; Lazić, V.; Rakić, D. Experimental-numerical study of tensile strength of the high-strength steel S690QL at elevated temperatures. *Strength Mater.* **2016**, *48*, 687–695. [CrossRef]
8. Arsić, D.; Lazić, V.; Sedmak, A.; Aleksandrović, S.; Živković, J.; Djordjević, M.; Mladenović, G. Effect of the elevated temperatures on mechanical properties of the ultra-high strength hot-work tool steel H11. *Trans. Famena* **2020**, *44*, 71–82. [CrossRef]

9. Ghafouri, M.; Amraei, M.; Pokka, A.-P.; Björk, T.; Larkiola, J.; Piili, H.; Zhao, X.-L. Mechanical properties of butt-welded ultra-high strength steels at elevated temperatures. *J. Constr. Steel Res.* **2022**, *198*, 107499. [CrossRef]
10. Amraei, M.; Ahola, A.; Afkhami, S.; Björk, T.; Heidarpour, A.; Zhao, X.L. Effects of heat input on the mechanical properties of butt-welded high and ultra-high strength steels. *Eng. Struct.* **2019**, *198*, 109460. [CrossRef]
11. Afkhami, S.; Björk, T.; Larkiol, J. Weldability of cold-formed high strength and ultra-high strength steels. *J. Constr. Steel Res.* **2019**, *158*, 86–98. [CrossRef]
12. Afkhami, S.; Skriko, T.; Lipiäinen, K.; Björk, T. Fracture, deformation route, and mechanical performance of welded cold-formed ultra-high strength steel S1100. *Procedia Struct. Integr.* **2024**, *61*, 53–61. [CrossRef]
13. Mandal, S.; Tewary, N.K.; Ghosh, S.K.; Chakrabarti, D.; Chatterjee, S. Thermo-mechanically controlled processed ultra high strength steel: Microstructure, texture and mechanical properties. *Mater. Sci. Eng. A* **2016**, *663*, 126–140. [CrossRef]
14. Javidan, F.; Heidarpour, A.; Zhao, X.L.; Hutchinson, C.R.; Minkkinen, J. Effect of weld on the mechanical properties of high strength and ultra-high strength steel tubes in fabricated hybrid sections. *Eng. Struct.* **2016**, *118*, 16–27. [CrossRef]
15. Moe, Y.A.; Hasib, M.T.; Paul, M.J.; Amraei, M.; Ahola, A.; Kruzic, J.; Heidarpour, A.; Zhao, X.L. Experimental study on the fatigue crack growth rates of welded ultra-high strength steel plates. *Adv. Struct. Eng.* **2023**, *26*, 2307–2324. [CrossRef]
16. Samardžić, I.; Ćorić, A.; Dunđer, M. Weldability investigation of fine-grained S1100QL steel. *Metalurgy* **2016**, *55*, 453–456.
17. Tümer, M.; Pixner, F.; Vallant, R.; Warchomicka, F.G.; Domitner, J.; Enzinger, N. Welding of S1100 Ultra high-Strength Steel Plates with Matching Metal-Cored Filler Wire: Microstructure, Residual Stresses, and Mechanical Properties, Steel. *Res. Int.* **2024**, *95*, 2300675. [CrossRef]
18. Liang, H.; Shi, X.; Li, Y. Effect of Ultrasonic Assistance on Properties of Ultra-High-Strength Steel in Laser-Arc Hybrid Welding. *Coatings* **2025**, *15*, 389. [CrossRef]
19. Available online: https://www.ssab.com/en/brands-and-products/strenx/product-offer/1100/e-f (accessed on 31 March 2025).
20. SSAB. *A Guide to Better Welding of HARDOX and STRENX, Welding Handbook*, 2nd ed.; SSAB: Oxelösund, Sweden, 2019; ISBN 978-91-978573-0-7.
21. Arsić, D.; Lazić, V.; Nikolić, R.R.; Sczygiol, N.; Krstić, B.; Ivković, D.J.; Hadzima, B.; Pastorek, F.; Ulewicz, R. Weldability Assessment of Various Steels by Hard-Facing. *Materials* **2022**, *15*, 3082. [CrossRef]
22. Jesenice, S.I.E. Catalog of Filler Materials. Available online: https://karikadoo.com/wp-content/uploads/2018/01/Jesenice-katalog.pdf (accessed on 25 November 2023). (In Serbian)
23. Available online: https://esab.com/lv/eur_en/products-solutions/product/filler-metals/low-alloy/mig-wires-tig-rods-gmaw-gtaw/ok-aristorod-89/ (accessed on 25 November 2023).
24. Christ, H.-J. Fatigue of Carbon and Alloy Steels. In *Encyclopedia of Materials: Science and Technology*; Buschow, K.H.J., Robert, C., Cahn, R., Merton, C.F., Bernhard, I., Edward, J.K., Subhash, M., Patrick, V., Eds.; Elsevier: Amsterdam, The Netherlands, 2001; pp. 2955–2963. [CrossRef]
25. Geng, L.; Tian, Z.; Sun, D.; Feng, X.; Zhang, F. Effects of Tempering Temperature on the Microstructure and Mechanical Properties of Vanadium-Microalloyed Medium-Carbon Bainitic Steel. *Coatings* **2025**, *15*, 503. [CrossRef]
26. Zachariah, S.A.; Shenoy, S.; Pai, D. Experimental analysis of the effect of the woven aramid fabric on the strain to failure behavior of plain weaved carbon/aramid hybrid laminates. *FACTA Univ. Ser. Mech. Eng.* **2024**, *22*, 13–24. [CrossRef]
27. Prijanovič, U.; Prijanovič, T.M.; Trdan, U.; Pleterski, M.; Jezeršek, M.; Klobčar, D. Remote Fibre Laser Welding of Advanced High Strength Martensitic Steel. *Metals* **2020**, *10*, 533. [CrossRef]
28. Younise, B.; Rakin, M.; Gubeljak, N.; Medjo, B.; Sedmak, A. Effect of material heterogeneity and constraint conditions on ductile fracture resistance of welded joint zones—Micromechanical assessment. *Eng. Fail. Anal.* **2017**, *82*, 435–445. [CrossRef]
29. Busari, Y.O.; Manurung, Y.H.P. Welded high strength low alloy steel influence on fatigue crack propagation using LEFM: A practical and thematic review. *Struct. Int. Life* **2020**, *20*, 263–279.